32nd Congress of the International Council of the Aeronautical Sciences
September 6-10, 2021
Pudong Shangri-La, Shanghai, China

TWISTOR BASED 6-DOF DISTRIBUTED ADAPTIVE LEADER-FOLLOWING CONTROL FOR MULTIPLE RIGID SPACECRAFT FORMATION

Bo Zhang[1], Fei Li[2] & Junqiang Bai[1]

[1]Northwestern Polytechnical University, Xi'an 710072, People's Republic of China
[2]China Academy of Launch Vehicle Technology, Beijing 100076, People's Republic of China

Abstract

In the recently developed twistor framework, the distributed control of six-degree-of-freedom (6-DOF) multiple spacecraft leader-following formation is investigated in the presence of unknown external disturbances. A distributed adaptive controller is proposed under an undirected communication graph to guarantee that the formation flying and consensus of the attitudes of the leader and followers is reached simultaneously. Firstly, the 6-DOF dynamics of a rigid spacecraft modeled by twistors is presented, and the distributed control problem is formulated. Then, a distributed sliding surface is established for the system composed of the kinematics of the spacecraft. Based on the sliding surface, a sliding mode controller for the 6-DOF formation is proposed. For the unknown disturbances, an adaptive law is developed to estimate the upper bounds to substitute for the unknowns in the sliding mode controller. The stability of the closed-loop system is proved via Lyapunov stability theory. Finally, the effectiveness of the proposed protocol is demonstrated by numerical simulations.

Keywords: twistor; 6-DOF spacecraft fomation; consensus control; distributed control; adaptive control

1. Introduction

Formation flying is capable of distributing the functionality of a conventional monolithic spacecraft to a group of small, low-cost, and cooperative spacecraft [1]. Spacecraft formation can reduce the risk of mission failure, enhance the versatility of spacecraft systems, eliminate the limitation of launch vehicles, and complete the tasks that need the cooperation of several spacecraft [1, 2]. Hence, the techniques for spacecraft formation have been extensive investigated.

As space tasks become more and more complex, not only are the positions of spacecraft required to form a specified pattern, but also their attitudes are expected to reach consensus simultaneously. Hence, the 6-DOF spacecraft formation has been drawing growing research interests. Kristiansen et al. [3] developed three nonlinear controllers for 6-DOF spacecraft formation on the basis of Euler–Lagrange system theory. Wang et al. [2, 4] investigated the control problem of 6-DOF leader-follower spacecraft formation in the framework of dual quaternions, and several sliding mode controllers were developed to ensure finite-time convergence in the presence of external disturbances. Ref. [5] addressed the problem of robust H_∞ control for 6-DOF formation flying with the translational and rotational coupling of the dynamics considered, and a modified $\theta - D$ method was proposed to solve the resultant Hamilton-Jacobi-Inequality. Sun et al. [6] investigated the control of both translational and rotational motions for small-satellite formation using only aerodynamic force; In the work, a novel coupled orbit-attitude model was established, based on which, a sliding mode controller was developed for the 6-DOF formation. In [7], a 6-DOF relative translation and rotation coupled dynamics model was represented by the exponential coordinates on the Lie group SE(3), and then an extended state observer was designed to eliminate the chattering of the proposed terminal sliding mode controller for the leader-following formation. Gao et al. [8] derived a dimensionless 6-DOF relative coupled dynamical model of the spacecraft in libration point orbits by using dual quaternions; Then, an active disturbance rejection controller was designed for the 6-DOF formation in libration point orbits. In Ref. [9], a fixed-time adaptive controller with quantized input was proposed for 6-DOF formation in the framework of dual quaternions. All of the above researches concentrate on the 6-DOF formation of only two spacecraft, the results of which are difficult to be used in multi-spacecraft formation with a certain communication topology among them.

Distributed control schemes do not require a control center to collect the information of all the other spacecraft, and 6-DOF formation can be achieved by only using the local measurements of each spacecraft and the information transmitted from its neighbors. If some of the formation-flying spacecraft malfunction, the rest spacecraft can still complete formation via a distributed control scheme. Consensus theory is an effective and powerful tool to design a distributed control scheme [10]. Ren [11] studied the control of formation keeping and attitude alignment for multiple spacecraft with a direct communication graph in the presence of arbitrary information loops or feedback between neighbors. However, in the study, it was assumed that the translational dynamics and rotational dynamics was decoupled. In [12], a collision-free distributed control scheme for 6-DOF spacecraft formation was proposed with the kinematics and dynamics represented by dual quaternions. In the design, the reference orbit and attitude information could only be obtained by a subset of the deputies, and a sliding mode controller was designed with the reference information estimated by a finite-time observer. In [13], with the Laplacian matrix of the communication graph of the spacecraft changing in accordance with a distance-based connectivity function between neighbors, an adaptive controller for the 6-DOF formation was proposed. Ref. [14] was devoted to the control problem of 6-DOF spacecraft formation with collision avoidance and network topology change. Huang et al. [15] studied the distributed adaptive finite-time synchronization control for 6-DOF formation without velocity measurements in the presence of external disturbances and parameter uncertainties.

The concept of twistors was from geometric algebra [16], and recently was employed to model 6-DOF relative motion of spacecraft [17, 18, 19, 20]. Twistors were first introduced to uniformly model relative pose motion of spacecraft to avoid the normalization constraint resulted from the dual quaternion representation [17]. Also, the twistor representation possesses a small-dimensional state, which can reduce computation and communication burdens for spacecraft with limited onboard resources. In [18], the authors developed an unscented Kalman filter for spacecraft pose estimation by using twistors. The work overcame the difficulty of unscented Kalman filter design using dual quaternions. Li et al. [19] developed a sliding mode controller for synchronization of the relative attitude and position of a separated ultraquiet spacecraft. Zhang et al. [20] proposed a twistor-based 6-DOF control scheme for the spacecraft landing on an asteroid, which could effectively enforce the LOS (line of sight) constraint and collision avoidance constraint.

In this paper, to ease the distributed controller design and lighten the computation and communication burden (transmitted fewer data) of 6-DOF formation, the twistor-based 6-DOF dynamic model is first used to develop a distributed adaptive controller for multi-spacecraft formation with an undirected communication graph. In the design, a sliding mode surface for the system composed of the kinematic of each spacecraft is proposed. Then, a distributed sliding mode backstepping control scheme is devised by the combination of the sliding mode control method and backstepping technique. For the unknown disturbances, an adaptive law is proposed to estimate the unknown upper bounds.

The remainder of this paper is organized as follows. Some preliminaries about quaternions, dual quaternions, twistors, and graph theory are presented in Section 2. The problem of 6-DOF spacecraft formation control is formulated in the framework of twistors in Section 3. The distributed adaptive controller is designed in Section 4. The results of numerical simulations are given in Section 5 to demonstrate the effectiveness of the controller. Finally, Section 6 concludes the paper.

2. Preliminaries

In this section, the definition and elementary operations of dual quaternions and twistors are introduced firstly. Then, some knowledge about graph theory is presented.

2.1 Quternions and Dual Quaternion

A quaternion is defined as $\boldsymbol{q} = q_1 i + q_2 j + q_3 k + q_4$, where $q_1, q_2, q_3, q_4 \in \mathbb{R}$, and $ij = -ji = k, jk = -kj = i, ki = -ik = j, i^2 = j^2 = k^2 = -1$ [21]. A quaternion can also be represented by the ordered pair $\boldsymbol{q} = (\bar{\boldsymbol{q}}, q_4)$ with $\bar{\boldsymbol{q}} \in \mathbb{R}^3$ being the vector part and $q_4 \in \mathbb{R}$ the scalar part. The sets of quaternions, vector quaternions, and scalar quaternions are denoted by $\mathbb{Q} = \{\boldsymbol{q}\,|\,\boldsymbol{q} = q_1 i + q_2 j + q_3 k + q_4, q_1, q_2, q_3, q_4 \in \mathbb{R}\}$, $\mathbb{Q}^v = \{\boldsymbol{q}\,|\,\boldsymbol{q} \in \mathbb{Q}, q_4 = 0\}$, and $\mathbb{Q}^s = \{\boldsymbol{q}\,|\,\boldsymbol{q} \in \mathbb{Q}, q_1 = q_2 = q_3 = 0\}$, respectively. The rotation about a unit vector $\boldsymbol{n}$ can be represented by the unit quaternion $\boldsymbol{q} = (\boldsymbol{n}\sin(\theta/2), \cos(\theta/2))$, where θ is the rotaion angle. Based on the definition of quaternions, a dual quaternion is defined as

$$\boldsymbol{p} = \boldsymbol{p}_r + \varepsilon \boldsymbol{p}_d,\ \boldsymbol{p}_r, \boldsymbol{p}_d \in \mathbb{Q} \tag{1}$$

where $\boldsymbol{p}_r$ and $\boldsymbol{p}_d$ are the real part and dual part of the dual quaternion, respectively. Similarly, the sets of dual quaternions, dual vector quaternions, and dual scalar quaternions are $\mathbb{D} = \{\boldsymbol{p}\,|\boldsymbol{p} = \boldsymbol{p}_r + \varepsilon\boldsymbol{p}_d,\ \boldsymbol{p}_r, \boldsymbol{p}_d \in \mathbb{Q}\}$, $\mathbb{D}^v = \{\boldsymbol{p}\,|\boldsymbol{p} = \boldsymbol{p}_r + \varepsilon\boldsymbol{p}_d,\ \boldsymbol{p}_r, \boldsymbol{p}_d \in \mathbb{Q}^v\}$, and $\mathbb{D}^s = \{\boldsymbol{p}\,|\boldsymbol{p} = \boldsymbol{p}_r + \varepsilon\boldsymbol{p}_d,\ \boldsymbol{p}_r, \boldsymbol{p}_d \in \mathbb{Q}^s\}$.

With the assumption $\boldsymbol{p}, \boldsymbol{q} \in \mathbb{D}$, some elementary algebraic operations on dual quaternions are shown as follows [20]:

Addition:

$$\boldsymbol{p} + \boldsymbol{q} = (\boldsymbol{p}_r + \boldsymbol{q}_r) + \varepsilon(\boldsymbol{p}_d + \boldsymbol{q}_d)$$

Multiplication by a scalar:

$$\lambda\boldsymbol{p} = \lambda\boldsymbol{p}_r + \varepsilon\lambda\boldsymbol{p}_d,\ \lambda \in \mathbb{R}$$

Multiplication:

$$\boldsymbol{p}\boldsymbol{q} = (\boldsymbol{p}_r\boldsymbol{q}_r) + \varepsilon(\boldsymbol{p}_r\boldsymbol{q}_d + \boldsymbol{p}_d\boldsymbol{q}_r)$$

Conjugation:

$$\boldsymbol{p}^* = \boldsymbol{p}_r^* + \varepsilon\boldsymbol{p}_d^*$$

where $\boldsymbol{p}_r^*$ and $\boldsymbol{p}_d^*$ are the conjugations of $\boldsymbol{p}_r$ and $\boldsymbol{p}_d$, respectively.

Inverse:

$$\frac{\mathbf{1}}{\boldsymbol{p}} = \frac{1}{\boldsymbol{p}_r^*\boldsymbol{p}_r}\boldsymbol{p}_r^* - \varepsilon\frac{1}{(\boldsymbol{p}_r^*\boldsymbol{p}_r)^2}\boldsymbol{p}_r^*\boldsymbol{p}_d\boldsymbol{p}_r^*$$

Division:

$$\frac{\boldsymbol{q}}{\boldsymbol{p}} = \frac{\mathbf{1}}{\boldsymbol{p}}\boldsymbol{q}$$

Swap:

$$\boldsymbol{p}^s = \boldsymbol{p}_d + \varepsilon\boldsymbol{p}_r$$

Cross product:

$$\boldsymbol{p} \times \boldsymbol{q} = \boldsymbol{p}_r \times \boldsymbol{q}_r + \varepsilon(\boldsymbol{p}_r \times \boldsymbol{q}_d + \boldsymbol{p}_d \times \boldsymbol{q}_r), \quad \boldsymbol{p}_r, \boldsymbol{q}_r \in \mathbb{D}^v$$

Circle product:

$$\boldsymbol{p} \circ \boldsymbol{q} = \boldsymbol{p}_r \cdot \boldsymbol{q}_r + \boldsymbol{p}_d \cdot \boldsymbol{q}_d$$

Multiplication by a matrix:

$$\boldsymbol{A}\boldsymbol{p} = (\boldsymbol{A}_{11}\boldsymbol{p}_r + \boldsymbol{A}_{12}\boldsymbol{p}_d) + \varepsilon(\boldsymbol{A}_{21}\boldsymbol{p}_r + \boldsymbol{A}_{22}\boldsymbol{p}_d)$$

where

$$\boldsymbol{A} = \begin{bmatrix} \boldsymbol{A}_{11} & \boldsymbol{A}_{12} \\ \boldsymbol{A}_{21} & \boldsymbol{A}_{22} \end{bmatrix}, \quad \boldsymbol{A}_{11}, \boldsymbol{A}_{12}, \boldsymbol{A}_{21}, \boldsymbol{A}_{22} \in \mathbb{R}^{4\times4}.$$

If a dual quaternion is regarded as a vector with four dual scalar quaternion elements, that is

$$\boldsymbol{p} = \begin{bmatrix} \bar{\boldsymbol{p}}_r + \varepsilon\bar{\boldsymbol{p}}_d \\ p_{r4} + \varepsilon p_{d4} \end{bmatrix} \in (\mathbb{D}^s)^{4\times1}$$

the following operation is defined:

$$\boldsymbol{A}\boldsymbol{p} = \begin{bmatrix} (\boldsymbol{A}_{11}\bar{\boldsymbol{p}}_r + \boldsymbol{A}_{12}p_{r4}) + \varepsilon(\boldsymbol{A}_{11}\bar{\boldsymbol{p}}_d + \boldsymbol{A}_{12}p_{d4}) \\ (\boldsymbol{A}_{21}\bar{\boldsymbol{p}}_r + \boldsymbol{A}_{22}p_{r4}) + \varepsilon(\boldsymbol{A}_{21}\bar{\boldsymbol{p}}_d + \boldsymbol{A}_{22}p_{d4}) \end{bmatrix}$$

where

$$\boldsymbol{A} = \begin{bmatrix} \boldsymbol{A}_{11} & \boldsymbol{A}_{12} \\ \boldsymbol{A}_{21} & \boldsymbol{A}_{22} \end{bmatrix} \in \mathbb{R}^{4\times4}, \quad \boldsymbol{A}_{11} \in \mathbb{R}^{3\times3},$$
$$\boldsymbol{A}_{12} \in \mathbb{R}^{3\times1},\ \boldsymbol{A}_{21} \in \mathbb{R}^{1\times3},\ \boldsymbol{A}_{22} \in \mathbb{R}$$

Deduced from the previous definitions, some useful properties are given below:

$$\boldsymbol{p}^s \circ \boldsymbol{q}^s = \boldsymbol{p} \circ \boldsymbol{q}, \quad \boldsymbol{p}, \boldsymbol{q} \in \mathbb{D}$$

$$(\boldsymbol{A}\boldsymbol{p}) \circ \boldsymbol{q} = \boldsymbol{p} \circ \left(\boldsymbol{A}^T\boldsymbol{q}\right), \quad \boldsymbol{p}, \boldsymbol{q} \in \mathbb{D},\ \boldsymbol{A} \in \mathbb{R}^{8\times8}$$

$$(\boldsymbol{AB})\boldsymbol{p} = \boldsymbol{A}(\boldsymbol{Bp}), \quad \boldsymbol{p},\boldsymbol{q} \in \mathbb{D},\ \boldsymbol{A},\boldsymbol{B} \in \mathbb{R}^{8\times 8}$$

$$\boldsymbol{p} \circ (\boldsymbol{q} + \boldsymbol{r}) = \boldsymbol{p} \circ \boldsymbol{q} + \boldsymbol{p} \circ \boldsymbol{r}, \quad \boldsymbol{p},\boldsymbol{q},\boldsymbol{r} \in \mathbb{D}$$

$$(\boldsymbol{pq})\boldsymbol{r} = \boldsymbol{p}(\boldsymbol{qr}), \quad \boldsymbol{p},\boldsymbol{q},\boldsymbol{r} \in \mathbb{D}$$

$$\boldsymbol{p} \circ (\boldsymbol{q} \times \boldsymbol{r}) = \boldsymbol{q}^s \circ (\boldsymbol{r} \times \boldsymbol{p}^s) = \boldsymbol{r}^s \circ (\boldsymbol{p}^s \times \boldsymbol{q}), \quad \boldsymbol{p},\boldsymbol{q},\boldsymbol{r} \in \mathbb{D}^v$$

According to the definition of the multiplication of two quaternions, one has [20]

$$\boldsymbol{pq} = [\boldsymbol{p}]\boldsymbol{q} = [\boldsymbol{q}]^{\vee}\boldsymbol{p}, \quad \boldsymbol{p},\boldsymbol{q} \in \mathbb{Q}, \tag{2}$$

where $[\boldsymbol{p}]$ and $[\boldsymbol{q}]^{\vee}$ represent 4×4 skew symmetric matrices related to $\boldsymbol{p}$ and $\boldsymbol{q}$ respectively, and they are given by

$$[\boldsymbol{p}] = \begin{bmatrix} p_4, & -p_3, & p_2, & p_1 \\ p_3, & p_4, & -p_1, & p_2 \\ -p_2, & p_1, & p_4, & p_3 \\ -p_1, & -p_2, & -p_3, & p_4 \end{bmatrix},$$

$$[\boldsymbol{q}]^{\vee} = \begin{bmatrix} q_4, & q_3, & -q_2, & q_1 \\ -q_3, & q_4, & q_1, & q_2 \\ q_2, & -q_1, & q_4, & q_3 \\ -q_1, & -q_2, & -q_3, & q_4 \end{bmatrix}.$$

For dual quaternions, there exists the similar transformation [20]:

$$\boldsymbol{pq} = [\boldsymbol{p}]\boldsymbol{q} = [\boldsymbol{q}]^{\vee}\boldsymbol{p}, \quad \boldsymbol{p},\boldsymbol{q} \in \mathbb{D}, \tag{3}$$

where

$$[\boldsymbol{p}] = \begin{bmatrix} [\boldsymbol{p}_r], & \boldsymbol{0}_{4\times 4} \\ [\boldsymbol{p}_d], & [\boldsymbol{p}_r] \end{bmatrix}, \quad [\boldsymbol{q}]^{\vee} = \begin{bmatrix} [\boldsymbol{q}_r]^{\vee}, & \boldsymbol{0}_{4\times 4} \\ [\boldsymbol{q}_d]^{\vee}, & [\boldsymbol{q}_r]^{\vee} \end{bmatrix}. \tag{4}$$

2.2 Graph Theory

In this paper, an undirected graph is used to describe the communication topology among the spacecraft. An undirected graph of order n is a pair $\mathcal{G} = (\mathcal{V},\mathcal{E})$, where $\mathcal{V} = \{v_1, v_2, \cdots, v_n\}$ is a finite nonempty node set and $\mathcal{E} = \mathcal{V}\times\mathcal{V}$ is an edge set of pairs of the nodes [10]. In the undirected graph $\mathcal{G}$, the edge (v_i, v_j) denotes that agents i and j can obtain information from each other. The weighted adjacent matrix of $\mathcal{G}$ is represented by $\boldsymbol{A} = [a_{ij}] \in \mathbb{R}^{n\times n}$, where $a_{ij} > 0$ if the pair of nodes $(i,j) \in \mathcal{E}$, $a_{ij} = 0$ otherwise. The Laplacia matrix $\boldsymbol{L} = [l_{ij}] \in \mathbb{R}^{n\times n}$ of $\mathcal{G}$ is defined as $l_{ii} = \sum_{j=1, j\neq i}^{n} a_{ij}$ and $l_{ij} = -a_{ij}, i \neq j$.

In spacecraft formation, it is assumed that there is a leader (or virtual leader), which is regarded as a node v_0 in the communication graph. The other spacecraft in the graph $\mathcal{G}$ are driven to follow the leader. Hence, the communication topology among the leader and the followers in $\mathcal{G}$ form a new augmented graph $\bar{\mathcal{G}}$. The access of the followers to the leader is represented by a diagonal matrix $\boldsymbol{B} = \mathrm{diag}(a_{10}, a_{20}, \cdots, a_{n0})$ [22]. If the $i-\mathrm{th}$ follower can receive information from the leader, $a_{i0} > 0$; otherwise, $a_{i0} = 0$.

Lemma 1 *If the undirected graph $\mathcal{G}$ is connected and at least one $a_{i0} > 0$, then $\boldsymbol{H} = \boldsymbol{L} + \boldsymbol{B}$ is symmetric positive definite [10].*

3. Problem Formulation

In 6-DOF formation, the body fixed frame of the $i-\mathrm{th}$ spacecraft is denoted as $\mathcal{F}_{B_i}$, whose origin O_{B_i} is located at the mass center of the $i-\mathrm{th}$ spacecraft, and axes coincide with the inertial principal axes to form a right-handed coordinate frame. The reference coordinate frame $\mathcal{L}_D$ is a local vertical local horizontal (LVLH) frame that moves on the reference orbit. The origin of $\mathcal{L}_D$ is the reference point on the orbit; its X_D-axis is in the orbit plane and points from the center of the Earth to the reference point; the Z_D-axis is perpendicular to the orbital plane and Y_D-axis point toward the moving direction of the reference point.

Express the relative position vector of the $i-\mathrm{th}$ spacecraft with respect to the reference point in the frame $\mathcal{F}_{B_i}$ as $\boldsymbol{r}_{B_iD}^{B_i}$. The relative attitude of the $i-\mathrm{th}$ spacecraft relative to $\mathcal{L}_D$ is represented by a quaternion $\boldsymbol{q}_{B_iD}$. Then the dual quaternion that can illustrate the relative pose of the $i-\mathrm{th}$ spacecraft with respect to the reference frame $\mathcal{L}_D$ is

$$\boldsymbol{p}_{B_iD} = \boldsymbol{q}_{B_iD} + \varepsilon\frac{1}{2}\boldsymbol{q}_{B_iD}\boldsymbol{r}^{B_i}_{B_iD} \in \mathbb{D} \tag{5}$$

Twistors were originally defined in the framework of geometric algebra [16], and were used to model the relative pose motion of spacecraft by Deng [17] and Zhang [20]. According to the definition of twistors in the framework of dual quaternions, the twistor corresponding to $\boldsymbol{p}_{B_iD}$ is

$$\boldsymbol{B}_i = \frac{\boldsymbol{p}_{B_iD} - \mathbf{1}}{\boldsymbol{p}_{B_iD} + \mathbf{1}} \in \mathbb{D}^v \tag{6}$$

The pose kinematics of the $i-\mathrm{th}$ spacecraft relative to the reference frame $\mathcal{L}_D$ is represented by [20]

$$\dot{\boldsymbol{B}}_i = \frac{1}{4}(\mathbf{1}+\boldsymbol{B}_i)\boldsymbol{V}_i(\mathbf{1}-\boldsymbol{B}_i) \in \mathbb{D}^v \tag{7}$$

where $\boldsymbol{V}_i = \boldsymbol{\omega}^{B_i}_{B_iD} + \varepsilon\left(\dot{\boldsymbol{r}}^{B_i}_{B_iD} + \boldsymbol{\omega}^{B_i}_{B_iD} \times \boldsymbol{r}^{B_i}_{B_iD}\right)$ with $\boldsymbol{\omega}^{B_i}_{B_iD}$ being the angular velocity of $\mathcal{F}_{B_i}$ relative to $\mathcal{F}_D$ expressed in $\mathcal{F}_{B_i}$. To describe the dynamics of $\mathcal{F}_{B_i}$ relative to $\mathcal{F}_D$, the standard Earth-centered inertial reference frame $\mathcal{F}_I$ is introduced. The relative dynamic equation is given by [20]

$$\begin{aligned}\dot{\boldsymbol{V}}_i =& \boldsymbol{M}^{-1}\left[\boldsymbol{F}^{B_i}_{g_i} + \boldsymbol{F}^{B_i}_{u_i} + \boldsymbol{F}^{B_i}_{d_i} - \boldsymbol{V}^{B_i}_{B_iI} \times \left(\boldsymbol{M}\boldsymbol{V}^{B_i}_{B_iI}\right)\right] - \frac{\mathbf{1}-\boldsymbol{B}_i}{\mathbf{1}+\boldsymbol{B}_i}\dot{\boldsymbol{V}}^D_{DI}\frac{\mathbf{1}+\boldsymbol{B}_i}{\mathbf{1}-\boldsymbol{B}_i} \\ &+ \boldsymbol{V}_i \times \left(\frac{\mathbf{1}-\boldsymbol{B}_i}{\mathbf{1}+\boldsymbol{B}_i}\boldsymbol{V}^D_{DI}\frac{\mathbf{1}+\boldsymbol{B}_i}{\mathbf{1}-\boldsymbol{B}_i}\right) \in \mathbb{D}^v\end{aligned} \tag{8}$$

where $\boldsymbol{V}^{B_i}_{B_iI} = \boldsymbol{\omega}^{B_i}_{B_iI} + \varepsilon\left(\dot{\boldsymbol{r}}^{B_i}_{B_iI} + \boldsymbol{\omega}^{B_i}_{B_iI} \times \boldsymbol{r}^{B_i}_{B_iI}\right)$ with $\boldsymbol{\omega}^{B_i}_{B_iI}$ and $\boldsymbol{r}^{B_i}_{B_iI}$ respectively being the angular velocity vector and position vector of $\mathcal{F}_{B_i}$ with respect to $\mathcal{F}_I$ expressed in $\mathcal{F}_{B_i}$. The expression of $\boldsymbol{V}^D_{d_i}$ is similar to $\boldsymbol{V}^{B_i}_{B_iI}$, and omitted here for conciseness.

The term $\boldsymbol{M}$ is called a dual inertia matrix, given by

$$\boldsymbol{M} = m\frac{\mathrm{d}}{\mathrm{d}\varepsilon}\boldsymbol{I}_3 + \varepsilon\boldsymbol{J} = \begin{bmatrix} m\frac{\mathrm{d}}{\mathrm{d}\varepsilon} + \varepsilon J_{11} & \varepsilon J_{12} & \varepsilon J_{13} \\ \varepsilon J_{12} & m\frac{\mathrm{d}}{\mathrm{d}\varepsilon} + \varepsilon J_{22} & \varepsilon J_{23} \\ \varepsilon J_{13} & \varepsilon J_{23} & m\frac{\mathrm{d}}{\mathrm{d}\varepsilon} + \varepsilon J_{33} \end{bmatrix} \tag{9}$$

where m is the mass of the spacecraft and J_{ij} $(i,j = 1,2,3)$ the elements of the inertial matrix $\boldsymbol{J}$. It is assumed that all the spacecraft possess the same mass and inertial matrix. $\boldsymbol{I}_3$ is a 3×3 identity matrix. Due to $\boldsymbol{B}_i, \boldsymbol{V}_i \in \mathbb{D}^v$, the scalar parts of them are discarded. Hence, the dimension of $\boldsymbol{M}$ is appropriate for matrix production. The inversion of $\boldsymbol{M}$ is

$$\boldsymbol{M}^{-1} = \boldsymbol{J}^{-1}\frac{\mathrm{d}}{\mathrm{d}\varepsilon} + \varepsilon\frac{1}{m}\boldsymbol{I}_3 \tag{10}$$

The term $\boldsymbol{F}^{B_i}_{g_i} = \boldsymbol{f}^{B_i}_{g_i} + \varepsilon\boldsymbol{\tau}^{B_i}_{g_i}$ is the force motor exerted on the $i-\mathrm{th}$ spacecraft expressed in $\mathcal{F}_{B_i}$. The gravitational force $\boldsymbol{f}^{B_i}_{g_i}$ is given by

$$\boldsymbol{f}^{B_i}_{g_i} = m\left(\boldsymbol{a}^{B_i}_{g_i} + \frac{\mathbf{1}+\boldsymbol{B}_{B_iI}}{\mathbf{1}-\boldsymbol{B}_{B_iI}}\boldsymbol{a}^I_{J_2}\frac{\mathbf{1}-\boldsymbol{B}_{B_iI}}{\mathbf{1}+\boldsymbol{B}_{B_iI}}\right) \tag{11}$$

where $\boldsymbol{a}^{B_i}_{g_i}$ is the gravitational acceleration caused by an ideal spherical Earth expressed in $\mathcal{F}_{B_i}$, and $\boldsymbol{a}^I_{J_2}$ is the perturbing acceleration due to Earth's oblateness expressed in $\mathcal{F}_I$. They are given by [21]

$$\boldsymbol{a}^{B_i}_{g_i} = -\mu\frac{\boldsymbol{r}^{B_i}_{B_iI}}{\|\boldsymbol{r}^{B_i}_{B_iI}\|^3} \tag{12}$$

$$\boldsymbol{a}^I_{J_2} = -\frac{3}{2}\frac{\mu J_2 R_e^2}{\|\boldsymbol{r}^I_{B_iI}\|^4}\begin{bmatrix} \left(1-5\left(\frac{z^I_{B_iI}}{\|\boldsymbol{r}^I_{B_iI}\|}\right)^2\right)\frac{x^I_{B_iI}}{\|\boldsymbol{r}^I_{B_iI}\|} \\ \left(1-5\left(\frac{z^I_{B_iI}}{\|\boldsymbol{r}^I_{B_iI}\|}\right)^2\right)\frac{y^I_{B_iI}}{\|\boldsymbol{r}^I_{B_iI}\|} \\ \left(3-5\left(\frac{z^I_{B_iI}}{\|\boldsymbol{r}^I_{B_iI}\|}\right)^2\right)\frac{z^I_{B_iI}}{\|\boldsymbol{r}^I_{B_iI}\|} \end{bmatrix} \tag{13}$$

where μ is the gravitational constant of the Earth, R_e the mean equatorial radius of the Earth. J_2 is a constant that describes the Earth's oblateness. The term $\boldsymbol{\tau}_{g_i}^{B_i}$ denotes the gravity gradient torque expressed in $\mathcal{F}_{B_i}$, which is given by

$$\boldsymbol{\tau}_{g_i}^{B_i} = \frac{3\mu \boldsymbol{r}_{B_i I}^{B_i}}{\|\boldsymbol{r}_{B_i I}^{B_i}\|^5} \times \boldsymbol{J}\boldsymbol{r}_{B_i I}^{B_i} \tag{14}$$

Rewrite $\boldsymbol{F}_{g_i}^{B_i}$ in a compact form, one obtains

$$\boldsymbol{F}_{g_i}^{B_i} = \boldsymbol{M}\boldsymbol{G}^{B_i} + \frac{3\mu \boldsymbol{R}_{B_i I}^{B_i}}{\|\boldsymbol{R}_{B_i I}^{B_i}\|^5} \times \boldsymbol{M}\boldsymbol{R}_{B_i I}^{B_i} \tag{15}$$

where $\boldsymbol{G}^{B_i} = \mathbf{0} + \varepsilon(\boldsymbol{a}_{g_i}^{B_i} + \boldsymbol{a}_{J_2}^{B})$, and $\boldsymbol{R}_{B_i I}^{B_i} = \boldsymbol{r}_{B_i I}^{B_i} + \varepsilon\mathbf{0}$. The term $\boldsymbol{F}_{u_i}^{B_i}$ is the control force motor expressed as $\boldsymbol{F}_{u_i}^{B_i} = \boldsymbol{f}_{u_i}^{B_i} + \varepsilon\boldsymbol{\tau}_{u_i}^{B_i}$, where $\boldsymbol{f}_{u_i}^{B_i}$ and $\boldsymbol{\tau}_{u_i}^{B_i}$ are control force and torque, respectively. $\boldsymbol{F}_{d_i}^{B_i}$ denotes the external disturbance force motor.
The pose error of the $i-\mathrm{th}$ follower relative to the leader is

$$\tilde{\boldsymbol{B}}_i = \boldsymbol{B}_i - \boldsymbol{B}_0 \tag{16}$$

The objective of the distributed adaptive pose control for 6-DOF formation in this paper is to design the control input $\boldsymbol{F}_{u_i}^{B_i}$ of the $i-\mathrm{th}$ spacecraft under a certain communication graph $\bar{\mathcal{G}}$ in the presence of unknown external disturbances, so that the followers establish formation flying with respect to the leader, and the attitudes of the followers are consistent with that of the leader simultaneously, that is

$$\lim_{t\to\infty} \tilde{\boldsymbol{B}}_i = \boldsymbol{\delta}_i \tag{17}$$

where $\boldsymbol{\delta}_i$ is a constant twistor, and the real part is $\mathbf{0}$, the dual part determined by the attitude of the leader and the desired formation.

4. Distributed Controller Design

This section is to design the distributed adaptive controller via the backstepping method. Before proceeding to the design, some assumptions are made as follows:

Assumption 1 *The communication graph $\mathcal{G}$ of the n follower spacecraft is undireccted and connected. At least one follower can obtain information from the leader.*

Assumption 2 *The disturbance force motor $\boldsymbol{F}_{d_i}^{B_i}$ is unknown but bounded by $|\boldsymbol{F}_{d_i}^{B_i}| \le \boldsymbol{D}_i \in \mathbb{D}^v$, which means that the absolute value of each element of $\boldsymbol{F}_{d_i}^{B_i}$ is less than or equal to the corresponding element of $\boldsymbol{D}_i$. The upper bound $\boldsymbol{D}_i$ is constant and unknown.*

According to Eq. (17), the pose error of the $i-\mathrm{th}$ follower relative to its desired pose is denoted by

$$\boldsymbol{e}_i = \boldsymbol{B}_i - \boldsymbol{\delta}_i - \boldsymbol{B}_0 \tag{18}$$

Considering the kinematics model (7), one gets the derivative of $\boldsymbol{e}_i$ as $\dot{\boldsymbol{e}}_i = \dot{\boldsymbol{B}}_i$. Therefore, the virtual control is given by

$$\boldsymbol{\alpha}_i = -\frac{4}{\mathbf{1}+\boldsymbol{B}_i}\boldsymbol{K}_\alpha \left\{ \sum_{j=1}^{n} a_{ij}\left[(\boldsymbol{B}_i - \boldsymbol{\delta}_i) - (\boldsymbol{B}_j - \boldsymbol{\delta}_j)\right] + a_{i0}(\boldsymbol{B}_i - \boldsymbol{\delta}_i - \boldsymbol{B}_0) \right\} \frac{1}{\mathbf{1}-\boldsymbol{B}_i} \tag{19}$$

where $\boldsymbol{K}_\alpha$ is a symmetric positive definite matrix. Choose the following Lyapunov function candidate

$$V_1 = \frac{1}{2}\sum_{i=1}^{n}\sum_{j=1}^{n} a_{ij}(\boldsymbol{e}_i - \boldsymbol{e}_j)\circ(\boldsymbol{e}_i - \boldsymbol{e}_j) + \sum_{i=1}^{n} a_{i0}\boldsymbol{e}_i \circ \boldsymbol{e}_i \tag{20}$$

The time derivative of V_1 is

$$\dot{V}_1 = \sum_{i=1}^{n}\sum_{j=1}^{n} a_{ij}(\dot{\boldsymbol{B}}_i - \dot{\boldsymbol{B}}_j)\circ\left[(\boldsymbol{B}_i - \boldsymbol{\delta}_i) - (\boldsymbol{B}_j - \boldsymbol{\delta}_j)\right] + 2\sum_{i=1}^{n} a_{i0}\dot{\boldsymbol{B}}_i \circ (\boldsymbol{B}_i - \boldsymbol{\delta}_i - \boldsymbol{B}_0)$$

$$
\begin{aligned}
&= 2\sum_{i=1}^{n}\sum_{j=1}^{n} a_{ij}\dot{\boldsymbol{B}}_i \circ \left[(\boldsymbol{B}_i-\boldsymbol{\delta}_i)-(\boldsymbol{B}_j-\boldsymbol{\delta}_j)\right] + 2\sum_{i=1}^{n} a_{i0}\dot{\boldsymbol{B}}_i \circ (\boldsymbol{B}_i-\boldsymbol{\delta}_i-\boldsymbol{B}_0) \\
&= 2\sum_{i=1}^{n}\dot{\boldsymbol{B}}_i \circ \left\{\sum_{j=1}^{n} a_{ij}\circ\left[(\boldsymbol{B}_i-\boldsymbol{\delta}_i)-(\boldsymbol{B}_j-\boldsymbol{\delta}_j)\right] + a_{i0}(\boldsymbol{B}_i-\boldsymbol{\delta}_i-\boldsymbol{B}_0)\right\} \\
&= 2\sum_{i=1}^{n}\left[\frac{1}{4}(\mathbf{1}+\boldsymbol{B}_i)\boldsymbol{V}_i(\mathbf{1}-\boldsymbol{B}_i)\right]\circ\left\{\sum_{j=1}^{n} a_{ij}\circ\left[(\boldsymbol{B}_i-\boldsymbol{\delta}_i)-(\boldsymbol{B}_j-\boldsymbol{\delta}_j)\right] + a_{i0}(\boldsymbol{B}_i-\boldsymbol{\delta}_i-\boldsymbol{B}_0)\right\}
\end{aligned} \tag{21}
$$

Replacing $\boldsymbol{V}_i$ with the virtual control $\boldsymbol{\alpha}_i$ yields

$$
\begin{aligned}
\dot{V}_1 &= -2\sum_{i=1}^{n}\boldsymbol{K}_\alpha\left\{\sum_{j=1}^{n} a_{ij}\circ\left[(\boldsymbol{B}_i-\boldsymbol{\delta}_i)-(\boldsymbol{B}_j-\boldsymbol{\delta}_j)\right] + a_{i0}(\boldsymbol{B}_i-\boldsymbol{\delta}_i-\boldsymbol{B}_0)\right\} \\
&\quad \circ\left\{\sum_{j=1}^{n} a_{ij}\circ\left[(\boldsymbol{B}_i-\boldsymbol{\delta}_i)-(\boldsymbol{B}_j-\boldsymbol{\delta}_j)\right] + a_{i0}(\boldsymbol{B}_i-\boldsymbol{\delta}_i-\boldsymbol{B}_0)\right\} \\
&= -2\left[(\boldsymbol{H}\otimes\boldsymbol{C})(\boldsymbol{B}-\boldsymbol{\delta}-\bar{\boldsymbol{B}}_0)\right]\circ\left[(\boldsymbol{H}\otimes\boldsymbol{C})(\boldsymbol{B}-\boldsymbol{\delta}-\bar{\boldsymbol{B}}_0)\right] \le 0
\end{aligned} \tag{22}
$$

where $\otimes$ represents Kronecker production of matrices, $\boldsymbol{B} = [\boldsymbol{B}_1, \boldsymbol{B}_2, \cdots, \boldsymbol{B}_n]^T \in \mathbb{R}^{8n\times1}$, $\boldsymbol{\delta} = [\boldsymbol{\delta}_1, \boldsymbol{\delta}_2, \cdots, \boldsymbol{\delta}_n]^T \in \mathbb{R}^{8n\times1}$, and $\bar{\boldsymbol{B}}_0 = [\boldsymbol{B}_0, \boldsymbol{B}_0, \cdots, \boldsymbol{B}_0]^T \in \mathbb{R}^{8n\times1}$. The matrix $\boldsymbol{C}$ satisfies $\boldsymbol{C}^T\boldsymbol{C} = \boldsymbol{K}_\alpha$. Recalling Assumption 1 and invoking Lemma 1, we know that $\boldsymbol{H}$ is symmetric positive definite, and therefore $\dot{V}_1$ is negative definite.
Let the error of the virtual control be

$$
\boldsymbol{Z}_i = \boldsymbol{V}_i - \boldsymbol{\alpha}_i \tag{23}
$$

Then, Eq. (7) can be rewritten as

$$
\dot{\boldsymbol{B}}_i = \frac{1}{4}(\mathbf{1}+\boldsymbol{B}_i)\boldsymbol{\alpha}_i(\mathbf{1}-\boldsymbol{B}_i) + \frac{1}{4}(\mathbf{1}+\boldsymbol{B}_i)\boldsymbol{Z}_i(\mathbf{1}-\boldsymbol{B}_i) \tag{24}
$$

The time derivative of V_1 becomes

$$
\begin{aligned}
\dot{V}_1 &= \frac{1}{2}\sum_{i=1}^{n}\left[(\mathbf{1}+\boldsymbol{B}_i)\boldsymbol{\alpha}_i(\mathbf{1}-\boldsymbol{B}_i) + (\mathbf{1}+\boldsymbol{B}_i)\boldsymbol{Z}_i(\mathbf{1}-\boldsymbol{B}_i)\right]\circ\left\{\sum_{j=1}^{n} a_{ij}\circ\left[(\boldsymbol{B}_i-\boldsymbol{\delta}_i)-(\boldsymbol{B}_j-\boldsymbol{\delta}_j)\right] + a_{i0}(\boldsymbol{B}_i-\boldsymbol{\delta}_i-\boldsymbol{B}_0)\right\} \\
&= \frac{1}{2}\sum_{i=1}^{n}\left[(\mathbf{1}+\boldsymbol{B}_i)\boldsymbol{\alpha}_i(\mathbf{1}-\boldsymbol{B}_i)\right]\circ\left\{\sum_{j=1}^{n} a_{ij}\circ\left[(\boldsymbol{B}_i-\boldsymbol{\delta}_i)-(\boldsymbol{B}_j-\boldsymbol{\delta}_j)\right] + a_{i0}(\boldsymbol{B}_i-\boldsymbol{\delta}_i-\boldsymbol{B}_0)\right\} \\
&\quad + \frac{1}{2}\sum_{i=1}^{n}\left[(\mathbf{1}+\boldsymbol{B}_i)\boldsymbol{Z}_i(\mathbf{1}-\boldsymbol{B}_i)\right]\circ\left\{\sum_{j=1}^{n} a_{ij}\circ\left[(\boldsymbol{B}_i-\boldsymbol{\delta}_i)-(\boldsymbol{B}_j-\boldsymbol{\delta}_j)\right] + a_{i0}(\boldsymbol{B}_i-\boldsymbol{\delta}_i-\boldsymbol{B}_0)\right\} \\
&= \frac{1}{2}\sum_{i=1}^{n}\left[(\mathbf{1}+\boldsymbol{B}_i)\boldsymbol{\alpha}_i(\mathbf{1}-\boldsymbol{B}_i)\right]\circ\left\{\sum_{j=1}^{n} a_{ij}\circ\left[(\boldsymbol{B}_i-\boldsymbol{\delta}_i)-(\boldsymbol{B}_j-\boldsymbol{\delta}_j)\right] + a_{i0}(\boldsymbol{B}_i-\boldsymbol{\delta}_i-\boldsymbol{B}_0)\right\} \\
&\quad + \frac{1}{2}\sum_{i=1}^{n}\boldsymbol{Z}_i\circ\left\{(\mathbf{1}+\boldsymbol{B}_i)^*\left\{\sum_{j=1}^{n} a_{ij}\circ\left[(\boldsymbol{B}_i-\boldsymbol{\delta}_i)-(\boldsymbol{B}_j-\boldsymbol{\delta}_j)\right] + a_{i0}(\boldsymbol{B}_i-\boldsymbol{\delta}_i-\boldsymbol{B}_0)\right\}^s(\mathbf{1}-\boldsymbol{B}_i)^*\right\}^s \\
&= -2\left[(\boldsymbol{H}\otimes\boldsymbol{C})(\boldsymbol{B}-\boldsymbol{\delta}-\bar{\boldsymbol{B}}_0)\right]\circ\left[(\boldsymbol{H}\otimes\boldsymbol{C})(\boldsymbol{B}-\boldsymbol{\delta}-\bar{\boldsymbol{B}}_0)\right] \\
&\quad - \frac{1}{8}\sum_{i=1}^{n}\boldsymbol{Z}_i\circ\left\{(\mathbf{1}+\boldsymbol{B}_i)^*\left[\boldsymbol{K}_\alpha^{-1}(\mathbf{1}+\boldsymbol{B}_i)\boldsymbol{\alpha}_i(\mathbf{1}-\boldsymbol{B}_i)\right]^s(\mathbf{1}-\boldsymbol{B}_i)^*\right\}^s
\end{aligned} \tag{25}
$$

Let

$$
\boldsymbol{Z}_i = \boldsymbol{K}_z\left\{(\mathbf{1}+\boldsymbol{B}_i)^*\left[\boldsymbol{K}_\alpha^{-1}(\mathbf{1}+\boldsymbol{B}_i)\boldsymbol{\alpha}_i(\mathbf{1}-\boldsymbol{B}_i)\right]^s(\mathbf{1}-\boldsymbol{B}_i)^*\right\}^s \tag{26}
$$

where $\boldsymbol{K}_z$ is symmetric positive definite. Substituting Eq. (26) into Eq. (25) results in

$$
\dot{V}_1 = -2\left[(\boldsymbol{H}\otimes\boldsymbol{C})(\boldsymbol{B}-\boldsymbol{\delta}-\bar{\boldsymbol{B}}_0)\right]\circ\left[(\boldsymbol{H}\otimes\boldsymbol{C})(\boldsymbol{B}-\boldsymbol{\delta}-\bar{\boldsymbol{B}}_0)\right]
$$

$$-\frac{1}{8}\sum_{i=1}^{n}\boldsymbol{K}_z\left\{(\mathbf{1}+\boldsymbol{B}_i)^*\left[\boldsymbol{K}_\alpha^{-1}(\mathbf{1}+\boldsymbol{B}_i)\alpha_i(\mathbf{1}-\boldsymbol{B}_i)\right]^s(\mathbf{1}-\boldsymbol{B}_i)^*\right\}^s$$
$$\circ\left\{(\mathbf{1}+\boldsymbol{B}_i)^*\left[\boldsymbol{K}_\alpha^{-1}(\mathbf{1}+\boldsymbol{B}_i)\alpha_i(\mathbf{1}-\boldsymbol{B}_i)\right]^s(\mathbf{1}-\boldsymbol{B}_i)^*\right\}^s\leq 0 \tag{27}$$

Eq. (27) indicates that $\lim_{t\to+\infty}\left(\boldsymbol{B}-\boldsymbol{\delta}-\bar{\boldsymbol{B}}_0\right)=\mathbf{0}$ when Eq. (26) holds. Hence, a sliding variable can be defined as

$$\boldsymbol{S}_i=\boldsymbol{Z}_i-\boldsymbol{K}_z\left\{(\mathbf{1}+\boldsymbol{B}_i)^*\left[\boldsymbol{K}_\alpha^{-1}(\mathbf{1}+\boldsymbol{B}_i)\alpha_i(\mathbf{1}-\boldsymbol{B}_i)\right]^s(\mathbf{1}-\boldsymbol{B}_i)^*\right\}^s \tag{28}$$

Theorem 1 *Consider the system consisting of one leader and n follower spacecraft with a communication graph $\bar{\mathcal{G}}$ that satisfies Assumption 1. The kinematics of each spacecraft is represented by Eq.* (7)*. The manifold $\{\mathfrak{R}\,|\boldsymbol{S}_i=\mathbf{0},\ i=1,2,\cdots,n\}$ is a sliding surface with $\alpha_i,\ i=1,2,\cdots,n$ given by Eq.* (19)*.*

Proof: The proof is straightorward from the previous analysis, therefore omitted here for conciseness. □

Remark 1 *It should be noted that the proposed sliding surface is determined by the combination of $\boldsymbol{S}_1=\mathbf{0},\boldsymbol{S}_2=\mathbf{0},\cdots,\boldsymbol{S}_n=\mathbf{0}$. A single manifold $\boldsymbol{S}_i=\mathbf{0}$ is not a sliding surface.*

Next, a distributed controller will be designed by the combination of the sliding mode control technique and backstepping method. The upper bound of the disturbance force motor $\boldsymbol{F}_d^{B_i}$ satisfies Assumption 2, and $\hat{\boldsymbol{D}}_i$ represents the estimate of $\boldsymbol{D}_i$. Then, the following adaptive 6-DOF distributed control scheme for the formation of multiple rigid spacecraft is proposed:

$$\begin{aligned}\boldsymbol{F}_u^{B_i}=&-\boldsymbol{K}_s\boldsymbol{S}_i^s-\hat{\boldsymbol{D}}_i\mathrm{sign}\left(\boldsymbol{S}_i^s\right)-\boldsymbol{F}_{g_i}^{B_i}+\boldsymbol{V}_{B_iI}^{B_i}\times\left(\boldsymbol{M}\boldsymbol{V}_{B_iI}^{B_i}\right)+\boldsymbol{M}\frac{\mathbf{1}-\boldsymbol{B}_i}{\mathbf{1}+\boldsymbol{B}_i}\dot{\boldsymbol{V}}_{DI}^{D}\frac{\mathbf{1}+\boldsymbol{B}_i}{\mathbf{1}-\boldsymbol{B}_i}\\&-\boldsymbol{M}\left[\boldsymbol{V}_i\times\left(\frac{\mathbf{1}-\boldsymbol{B}_i}{\mathbf{1}+\boldsymbol{B}_i}\boldsymbol{V}_{DI}^{D}\frac{\mathbf{1}+\boldsymbol{B}_i}{\mathbf{1}-\boldsymbol{B}_i}\right)\right]+\boldsymbol{M}\dot{\alpha}+\boldsymbol{M}\left(\boldsymbol{K}_z\dot{\boldsymbol{Y}}_i\right)+\frac{1}{8}\boldsymbol{Y}_i^s\end{aligned} \tag{29}$$

where $\boldsymbol{Y}_i=\left\{(\mathbf{1}+\boldsymbol{B}_i)^*\left\{\boldsymbol{K}_\alpha^{-1}(\mathbf{1}+\boldsymbol{B}_i)\alpha_i(\mathbf{1}-\boldsymbol{B}_i)\right\}^s(\mathbf{1}-\boldsymbol{B}_i)^*\right\}^s$. The expressions of $\dot{\alpha}_i$ and $\dot{\boldsymbol{Y}}_i$ are given in Appendix. The adaptive law for estimating $\boldsymbol{D}_i$ is

$$\dot{\hat{\boldsymbol{D}}}_i=\boldsymbol{K}_d^{-1}\left|\boldsymbol{S}_i^s\right| \tag{30}$$

where $\boldsymbol{K}_d$ is a symmetric positive definite matrix.

Theorem 2 *Consider the system consisting of one leader and n follower spacecraft with a communication graph $\bar{\mathcal{G}}$ that satisfies Assumption 1. The kinematics of each spacecraft is represented by Eq.* (7)*, dynamics represented by Eq.* (8) *with the disturbance force motor meeting Assumption 2. Then, the positions of the followers form a specified formation relative to the leader and the attitudes of the followers are consistent with the leader under the distributed adaptive control scheme composed of Eqs.* (29) *and* (30)*. In addition, the estimate of $\boldsymbol{D}_i$ is bounded.*

Proof: Consider the Lyapunov function candidate

$$V_2=V_1+\frac{1}{2}\sum_{i=1}^{n}\boldsymbol{S}_i^s\circ\boldsymbol{M}\boldsymbol{S}_i+\frac{1}{2}\sum_{i=1}^{n}\tilde{\boldsymbol{D}}_i\circ\boldsymbol{K}_d\tilde{\boldsymbol{D}}_i \tag{31}$$

where $\tilde{\boldsymbol{D}}_i=\hat{\boldsymbol{D}}_i-\boldsymbol{D}_i$. Differeniating V_2 with respect to time yields

$$\begin{aligned}\dot{V}_2=&\dot{V}_1+\sum_{i=1}^{n}\boldsymbol{S}_i^s\circ\boldsymbol{M}\dot{\boldsymbol{S}}_i+\sum_{i=1}^{n}\tilde{\boldsymbol{D}}_i\circ\boldsymbol{K}_D\dot{\hat{\boldsymbol{D}}}_i\\=&-2\left[(\boldsymbol{H}\otimes\boldsymbol{C})\left(\boldsymbol{B}-\boldsymbol{\delta}-\bar{\boldsymbol{B}}_0\right)\right]\circ\left[(\boldsymbol{H}\otimes\boldsymbol{C})\left(\boldsymbol{B}-\boldsymbol{\delta}-\bar{\boldsymbol{B}}_0\right)\right]\\&-\frac{1}{8}\sum_{i=1}^{n}\left\{\boldsymbol{S}_i+\boldsymbol{K}_z\boldsymbol{Y}_i\right\}\circ\boldsymbol{Y}_i+\sum_{i=1}^{n}\boldsymbol{S}_i^s\circ\boldsymbol{M}\left(\dot{\boldsymbol{V}}_i-\dot{\alpha}_i-\boldsymbol{K}_z\dot{\boldsymbol{Y}}_i\right)+\sum_{i=1}^{n}\tilde{\boldsymbol{D}}\circ\left|\boldsymbol{S}_i^s\right|\end{aligned} \tag{32}$$

Substituting the control law Eq. (29) and adaptive law Eq. (30) into Eq. (32) with some algebraic operations leads to

$$\begin{aligned}
\dot{V}_2 =& -2\left[(\boldsymbol{H}\otimes\boldsymbol{C})\left(\boldsymbol{B}-\boldsymbol{\delta}-\bar{\boldsymbol{B}}_0\right)\right]\circ\left[(\boldsymbol{H}\otimes\boldsymbol{C})\left(\boldsymbol{B}-\boldsymbol{\delta}-\bar{\boldsymbol{B}}_0\right)\right]\\
&-\frac{1}{8}\sum_{i=1}^{n}\boldsymbol{K}_z\boldsymbol{Y}_i\circ\boldsymbol{Y}_i-\frac{1}{8}\sum_{i=1}^{n}\boldsymbol{S}_i\circ\boldsymbol{Y}_i+\sum_{i=1}^{n}\boldsymbol{S}_i^s\circ\left[\frac{1}{8}\boldsymbol{Y}_i^s-\boldsymbol{K}_s\boldsymbol{S}_i^s-\hat{\boldsymbol{D}}_i\mathrm{sign}\left(\boldsymbol{S}_i^s\right)+\boldsymbol{F}_{d_i}^{B_i}\right]+\sum_{i=1}^{n}\tilde{\boldsymbol{D}}\circ\left|\boldsymbol{S}_i^s\right|\\
\le& -2\left[(\boldsymbol{H}\otimes\boldsymbol{C})\left(\boldsymbol{B}-\boldsymbol{\delta}-\bar{\boldsymbol{B}}_0\right)\right]\circ\left[(\boldsymbol{H}\otimes\boldsymbol{C})\left(\boldsymbol{B}-\boldsymbol{\delta}-\bar{\boldsymbol{B}}_0\right)\right]\\
&-\frac{1}{8}\sum_{i=1}^{n}\boldsymbol{K}_z\boldsymbol{Y}_i\circ\boldsymbol{Y}_i+\sum_{i=1}^{n}\boldsymbol{S}_i^s\circ\left[-\boldsymbol{K}_s\boldsymbol{S}_i^s-\hat{\boldsymbol{D}}_i\mathrm{sign}\left(\boldsymbol{S}_i^s\right)+\boldsymbol{F}_{d_i}^{B_i}\right]+\sum_{i=1}^{n}\tilde{\boldsymbol{D}}\circ\left|\boldsymbol{S}_i^s\right|\\
\le& -2\left[(\boldsymbol{H}\otimes\boldsymbol{C})\left(\boldsymbol{B}-\boldsymbol{\delta}-\bar{\boldsymbol{B}}_0\right)\right]\circ\left[(\boldsymbol{H}\otimes\boldsymbol{C})\left(\boldsymbol{B}-\boldsymbol{\delta}-\bar{\boldsymbol{B}}_0\right)\right]\\
&-\frac{1}{8}\sum_{i=1}^{n}\boldsymbol{K}_z\boldsymbol{Y}_i\circ\boldsymbol{Y}_i-\sum_{i=1}^{n}\boldsymbol{S}_i^s\circ\left(\boldsymbol{K}_s\boldsymbol{S}_i^s\right)\\
\le& 0
\end{aligned} \tag{33}$$

It is obvious that V_2 is positive semi-definite, and therefore $\boldsymbol{B},\boldsymbol{S}_1,\boldsymbol{S}_2,\cdots,\boldsymbol{S}_n,\tilde{\boldsymbol{D}}_1,\tilde{\boldsymbol{D}}_2,\cdots,\tilde{\boldsymbol{D}}_n\in\mathcal{L}_\infty$. Because V_2 is radially unbounded, there exist a constant scalar ε to render the set $\boldsymbol{\Omega}=\left\{\boldsymbol{B},\boldsymbol{S}_1,\boldsymbol{S}_2,\cdots,\boldsymbol{S}_n,\tilde{\boldsymbol{D}}_1,\tilde{\boldsymbol{D}}_2,\cdots,\tilde{\boldsymbol{D}}_n \mid V_2<\varepsilon\right\}$ compact and positively invariant with respect to the closed-loop system. Let $\boldsymbol{E}$ be the set of all points in Ω where $\dot{V}_2=0$, i.e.

$$\boldsymbol{E}=\left\{\boldsymbol{B}-\boldsymbol{\delta}-\bar{\boldsymbol{B}}_0=\boldsymbol{0},\boldsymbol{Y}_1=\boldsymbol{0},\boldsymbol{Y}_2=\boldsymbol{0},\cdots,\boldsymbol{Y}_n=\boldsymbol{0},\boldsymbol{S}_1=\boldsymbol{0},\boldsymbol{S}_2=\boldsymbol{0},\cdots,\boldsymbol{S}_n=\boldsymbol{0}\right\} \tag{34}$$

Obviously, the largest invariant set in $\boldsymbol{E}$ is $\boldsymbol{\Gamma}=\boldsymbol{E}$. Invoking LaSalle's theorem [23], we know that every solution starting in $\boldsymbol{\Omega}$ approaches $\boldsymbol{\Gamma}$ as $t\to\infty$. Hence,

$$\lim_{t\to\infty}\boldsymbol{B}-\boldsymbol{\delta}-\bar{\boldsymbol{B}}_0=\boldsymbol{0} \tag{35}$$

which means the 6-DOF formation of the spacecraft is established. The proof is completed. □

In the sliding mode controller, the sign function results in control input chattering. To avoid the problem, the sigmoid function can be used to approximate the sign function [24]. The sigmoid function is defined as

$$\mathrm{sigmoid}(x)=\frac{x}{|x|+\Delta} \tag{36}$$

where Δ is a small positive scalar. With the sign function replaced with Eq. (36), $\boldsymbol{B}-\boldsymbol{\delta}-\bar{\boldsymbol{B}}_0$ only converges to the neighborhood of $\boldsymbol{0}$.

5. Simulations

An illustrative simulation example is given in this section. The number of the followers is set to 5, and the 1st follower can obtain information from the leader. The communication topology is given by the graph in Figure 1. The weighted adjacency matrix of the communication graph of the followers is

$$\boldsymbol{A}=\begin{bmatrix}0&1&1&0&0\\1&0&0&1&0\\1&0&0&0&1\\0&1&0&0&0\\0&0&1&0&0\end{bmatrix}\times10^{-8} \tag{37}$$

The matrix representing the information access of the follower to the leader is given by

$$\boldsymbol{B}=\begin{bmatrix}1&0&0&0&0\\0&0&0&0&0\\0&0&0&0&0\\0&0&0&0&0\\0&0&0&0&0\end{bmatrix}\times10^{-8} \tag{38}$$

It is assumed that all the spacecraft possess the same mass and inertial matrix, which are

$$m = 50\ \mathrm{kg},\ \boldsymbol{J} = \begin{bmatrix} 22 & 1 & 0.5 \\ 1 & 20 & 0.8 \\ 0.5 & 0.8 & 25 \end{bmatrix} \mathrm{kg}\cdot\mathrm{m}^2 \tag{39}$$

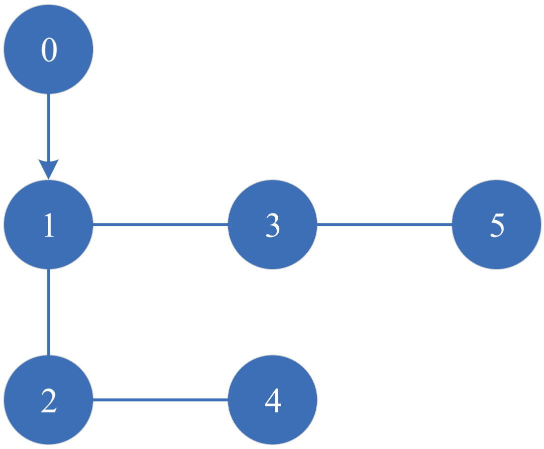

Figure 1 – Communication topology.

The reference orbit is a low Earth orbit, whose elements are given in Table 1. The origin of the LVLH coordinate frame $\mathcal{L}_D$ is fixed on the point that moves along the reference orbit. The relative position vector of the leader with respect to $\mathcal{L}_D$ expressed in $\mathcal{L}_D$ is $\boldsymbol{r}^D_{B_0D} = [10,\ 20,\ 10]^T$ m, and the relative velocity is $\dot{\boldsymbol{r}}^D_{B_0D} = [0,\ 0,\ 0]^T$ m/s. The attitude of the leader relative to $\mathcal{L}_D$ is represented by the quaternion $\boldsymbol{q}_{B_0D} = [\sin(\pi/3),\ 0,\ 0,\ \cos(\pi/3)]^T$, and the relative angular velocity expressed in $\mathcal{L}_D$ is $\omega^D_{B_0D} = [0,\ 0,\ 0]^T$ rad/s. From the setting, we know that the leader is fixed in the reference frame $\mathcal{L}_D$. The initial relative positions, velocities, quaternions, and angular velocities of the followers relative to the frame $\mathcal{L}_D$ expressed in $\mathcal{L}_D$ are given in Table 2. The initial value of $\boldsymbol{B}_i$ and $\boldsymbol{V}_i$ can be calculated according to the definitions. The desired relative positions of the followers relative to the leader expressed in $\mathcal{L}_D$ is set to the values shown in Table 3 to form a regular pentagon.

Table 1 – Orbital elements of the leader.

Parameter	Perigee altitude	Eccentricity	RAAN	Inclination	Argument of perigee	True anomaly
Value	500 km	0	50 deg	45 deg	30deg	10 deg

Table 2 – Initial states of the followers.

Spacecraft	Initial position $\boldsymbol{r}^D_{B_iD}$	Initial velocity $\dot{\boldsymbol{r}}^D_{B_iD}$
1	$[4.4943,\ 200.4371,\ 97.2679]^T$ m	$[0,\ 0,\ 0]^T$ m/s
2	$[-69.0684,\ 70.8708,\ 112.1265]^T$ m	$[0,\ 0,\ 0]^T$ m/s
3	$[76.4665,\ -102.2596,\ 85.6776]^T$ m	$[0,\ 0,\ 0]^T$ m/s
4	$[161.4337,\ -36.8823,\ 38.2923]^T$ m	$[0,\ 0,\ 0]^T$ m/s
5	$[166.6738,\ 172.8339,\ 56.6358]^T$ m	$[0,\ 0,\ 0]^T$ m/s
	Initial quaternion $\boldsymbol{q}_{B_iD}$	Initial angular velocity $\omega^D_{B_iD}$
1	$[0.6088,\ 0.2227,\ 0.5483,\ 0.5284]^T$	$[0,\ 0,\ 0]^T$ rad/s
2	$[0.1478,\ 0.1082,\ 0.4530,\ 0.8725]^T$	$[0,\ 0,\ 0]^T$ rad/s
3	$[0.3286,\ 0.5650,\ 0.2161,\ 0.7253]^T$	$[0,\ 0,\ 0]^T$ rad/s
4	$[0.2015,\ 0.3996,\ 0.5521,\ 0.7036]^T$	$[0,\ 0,\ 0]^T$ rad/s
5	$[0.8542,\ 0.4873,\ 0.1234,\ 0.1329]^T$	$[0,\ 0,\ 0]^T$ rad/s

The control gain matrices $\boldsymbol{K}_\alpha$, $\boldsymbol{K}_s$, $\boldsymbol{K}_z$, and $\boldsymbol{K}_d^{-1}$ are set to $\boldsymbol{K}_\alpha = \mathrm{diag}([0.5,\ 0.5,\ 0.5,\ 0.5,\ 1,\ 1,\ 1,\ 1]) \times 10^7$, $\boldsymbol{K}_s = \mathrm{diag}([1,\ 1,\ 1,\ 1,\ 5,\ 5,\ 5,\ 5])$, $\boldsymbol{K}_z = \mathrm{diag}([1,\ 1,\ 1,\ 1,\ 2,\ 2,\ 2,\ 2])$, and $\boldsymbol{K}_d^{-1} = \mathrm{diag}\big(\big[1\times10^{-4},\ 1\times10^{-4},\ 1\times10^{-4},$

Table 3 – Desired formation position.

Spacecraft	Desired position relative to the leader
1	$\delta_{r_1}^D = [-60.5057,\ 135.4371,\ 22.2679]^T$ m
2	$\delta_{r_2}^D = [-144.0684,\ -19.1292,\ 37.1265]^T$ m
3	$\delta_{r_3}^D = [-28.5335,\ -147.2596,\ 0.6776]^T$ m
4	$\delta_{r_4}^D = [126.4337,\ -71.8823,\ -36.7077]^T$ m
5	$\delta_{r_5}^D = [106.6738,\ 102.8339,\ -23.3642]^T$ m

$1\times 10^{-4},\ 1,\ 1,\ 1,\ 1])\times 10^{-2}$, respectively. The external disturbances are given as

$$f_d^{B_i} = \left(\begin{bmatrix} 2\sin(0.1t)+0.2\sin\left(t+\frac{\pi}{2}\right) \\ 5\sin\left(0.1t+\frac{\pi}{4}\right)+0.5\sin\left(t+\frac{\pi}{4}\right) \\ 4\sin\left(0.1t+\frac{\pi}{2}\right)+0.4\sin(t) \end{bmatrix} + \begin{bmatrix} 4 \\ 3 \\ -5 \end{bmatrix}\right)\times 10^{-4}\ \mathrm{N}$$

$$\tau_d^{B_i} = \left(\begin{bmatrix} 6\sin(0.5t)+0.6\sin\left(5t+\frac{\pi}{2}\right) \\ 3\sin\left(0.5t+\frac{\pi}{4}\right)+0.3\sin\left(5t+\frac{\pi}{4}\right) \\ 4\sin\left(0.5t+\frac{\pi}{2}\right)+0.4\sin(5t) \end{bmatrix} + \begin{bmatrix} -2 \\ 5 \\ 4 \end{bmatrix}\right)\times 10^{-4}\ \mathrm{N\cdot m}$$

The position errors of the followers are shown in Figure 2. It is obvious that all the followers converge to their desired positions to fly in formation with the specified pattern. The convergence of the 1st follower is the fastest because it can directly access the leader. Though only the 1st follower can obtain the information of the leader, the other followers reach their each desired position relative to the leader. The 3-dimensional trajectories of the followers are plotted in Figure 3. As can be seen, the regular pentagon formation is accurately established.

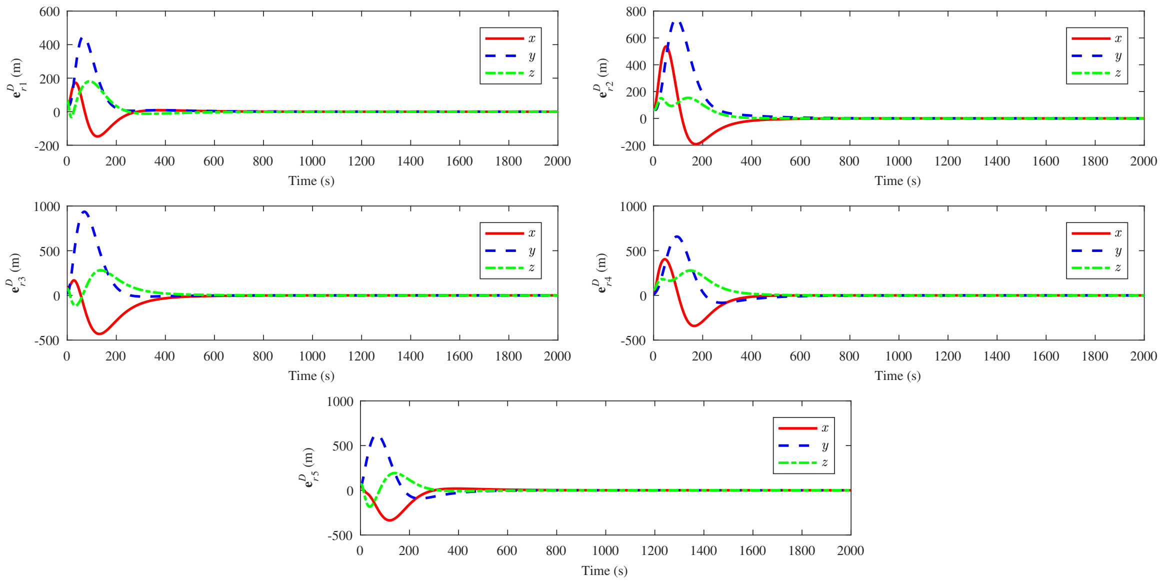

Figure 2 – The position error histories of the followers in the frame $\mathcal{F}_D$.

The consensus of the spacecraft's attitude is presented in Figure 4. All the errors of the real parts of the twistors reach the neighborhood of zero in about 600s, though the attitudes of the followers are randomly initialized. It should be noted that the real parts of twistors is just 3-dimensional, which is different from dual quaternions.
The histories of the control force and control torque are shown in Figures 5 and 6. It can be observed that the control force increases rapidly despite the fact that the relative position between each follower and the leader has been almost unchanging, the reason of which is that the leader are actually orbiting around the Earth and the periodic control force (the periodic time is too long to demonstrate the periodicity in the Figures) has to be exerted on the followers to keep the formation. The attitude of the leader varies slowly, so just small control torque is needed to ensure the attitude consensus.

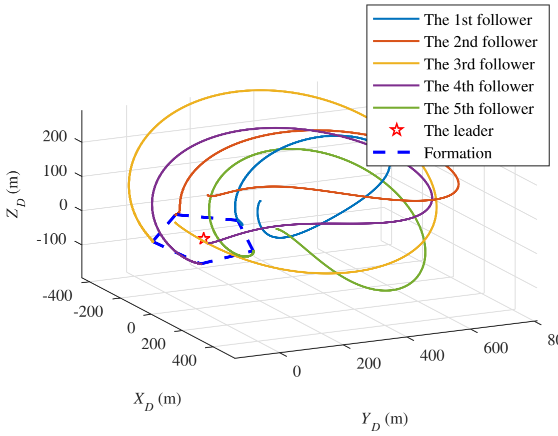

Figure 3 – The trajectories of the followers in the frame $\mathcal{F}_D$.

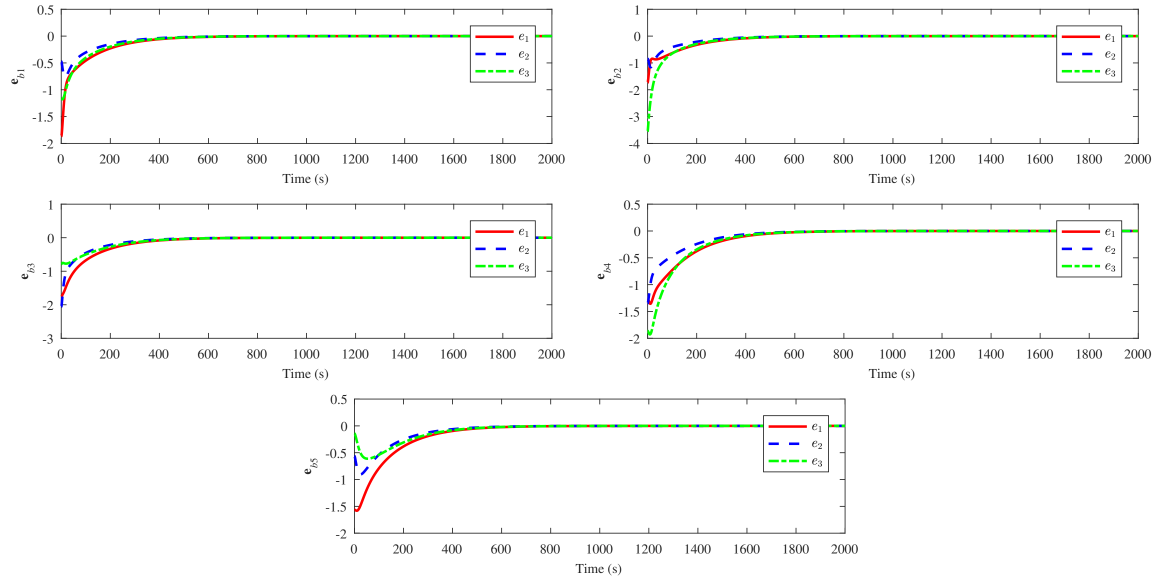

Figure 4 – The attitude error histories of the followers.

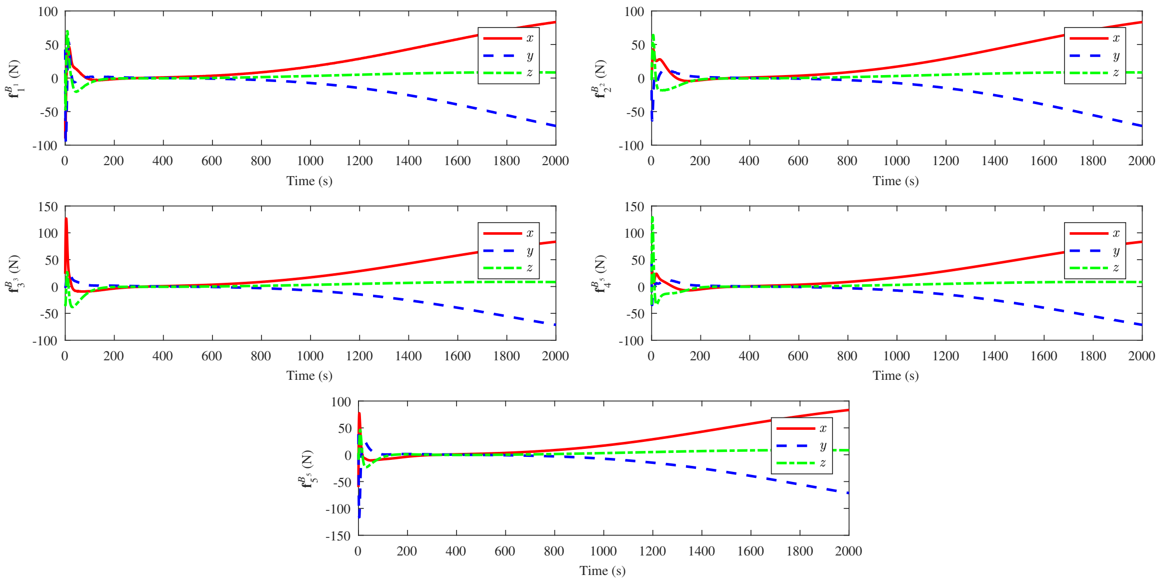

Figure 5 – The control force histories of the followers.

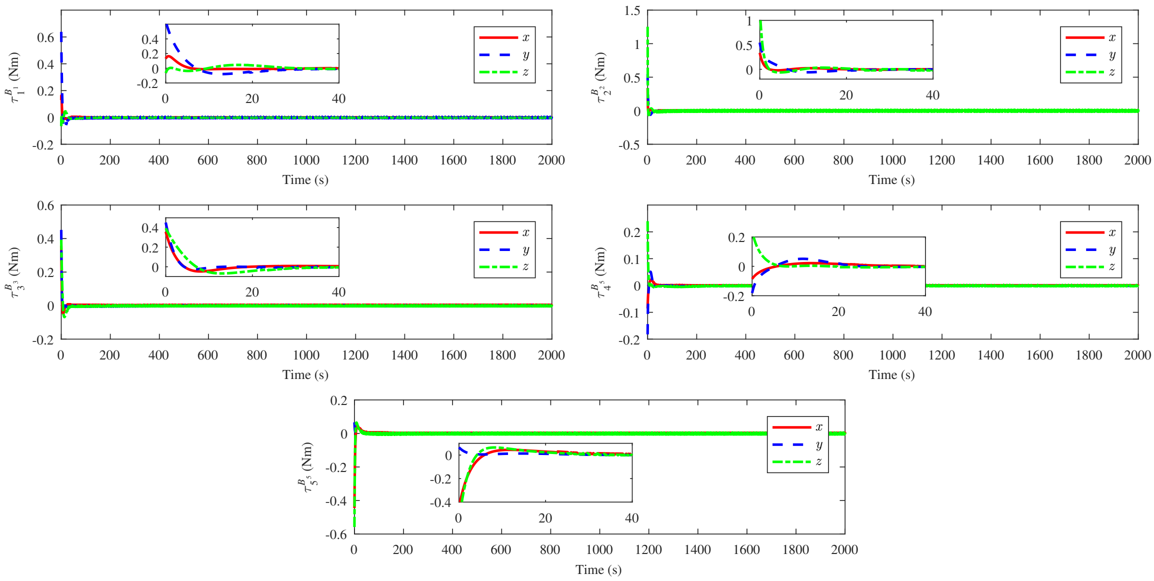

Figure 6 – The control torque histories of the followers.

6. Conclusion

A distributed adaptive controller for 6-DOF leader-following multi-spacecraft formation is proposed in the framework of twistors. Based on the consensus theory and backstepping technique, a distributed virtual control law for each follower spacecraft is devised under the assumption that the communication topology of the followers is a connected undirected graph and at least one follower can access the leader. Then, a sliding surface is proposed for the system consisting of the kinematics of all the followers. By the application of the sliding surface, a backstepping sliding mode control scheme is developed with the unknown upper bound of the external disturbance force motor estimated by an adaptive law. The stability of the whole closed-loop system is proved and numerical simulations demonstrate the effectiveness of the proposed algorithm. Compared with the distributed pose controller based on dual quaternions, our work provides a more efficient solution to the distributed control of 6-DOF multi-spacecraft formation because the transmitted states of the spacecraft possess smaller dimensions. To further lighten the communication burden, an event-triggering mechanism can be considered in future studies.

7. Acknowledgment

This work was supported by the National Natural Science Foundation of China (Grant No. 62003268) and the Fundamental Research Funds for the Central Universities (Grant No. G2020KY0503). The authors greatly appreciate the financial support.

8. Contact Author Email Address

The email of the contact author is npuzhbo@163.com.

9. Copyright Statement

Appendix: Expressions of $\dot{\alpha}_i$ and $\dot{Y}_i$

The expansions of $\dot{\boldsymbol{\alpha}}_i$ is given as follows:

$$\dot{\boldsymbol{\alpha}}_i = \frac{4}{\boldsymbol{1}+\boldsymbol{B}_i}\dot{\boldsymbol{B}}_i\frac{1}{\boldsymbol{1}+\boldsymbol{B}_i}\boldsymbol{K}_\alpha\left\{\sum_{j=1}^{n} a_{ij}\left[(\boldsymbol{B}_i-\boldsymbol{\delta}_i)-(\boldsymbol{B}_j-\boldsymbol{\delta}_j)\right]+a_{i0}\left(\boldsymbol{B}_i-\boldsymbol{\delta}_i-\boldsymbol{B}_0\right)\right\}\frac{1}{\boldsymbol{1}-\boldsymbol{B}_i}$$

$$+\frac{4}{\mathbf{1}+\boldsymbol{B}_i}\boldsymbol{K}_\alpha\left[\sum_{j=1}^{n}a_{ij}\left(\dot{\boldsymbol{B}}_i-\dot{\boldsymbol{B}}_j\right)+a_{i0}\dot{\boldsymbol{B}}_i\right]\frac{1}{\mathbf{1}-\boldsymbol{B}_i}$$
$$-\frac{4}{\mathbf{1}+\boldsymbol{B}_i}\boldsymbol{K}_\alpha\left\{\sum_{j=1}^{n}a_{ij}\left[(\boldsymbol{B}_i-\boldsymbol{\delta}_i)-\left(\boldsymbol{B}_j-\boldsymbol{\delta}_j\right)\right]+a_{i0}\left(\boldsymbol{B}_i-\boldsymbol{\delta}_i-\boldsymbol{B}_0\right)\right\}\frac{1}{\mathbf{1}-\boldsymbol{B}_i}\dot{\boldsymbol{B}}_i\frac{1}{\mathbf{1}-\boldsymbol{B}_i}$$

where $\dot{\boldsymbol{B}}_i$ is given by Eq. (7). The term $\dot{\boldsymbol{Y}}_i$ is

$$\dot{\boldsymbol{Y}}_i=\left\{\left(\dot{\boldsymbol{B}}_i\right)^*\left\{\boldsymbol{K}_\alpha^{-1}\left(\mathbf{1}+\boldsymbol{B}_i\right)\alpha_i\left(\mathbf{1}-\boldsymbol{B}_i\right)\right\}^s\left(\mathbf{1}-\boldsymbol{B}_i\right)^*\right\}^s+\left\{\left(\mathbf{1}+\boldsymbol{B}_i\right)^*\left\{\boldsymbol{K}_\alpha^{-1}\dot{\boldsymbol{B}}_i\alpha_i\left(\mathbf{1}-\boldsymbol{B}_i\right)\right\}^s\left(\mathbf{1}-\boldsymbol{B}_i\right)^*\right\}^s$$
$$+\left\{\left(\mathbf{1}+\boldsymbol{B}_i\right)^*\left\{\boldsymbol{K}_\alpha^{-1}\left(\mathbf{1}+\boldsymbol{B}_i\right)\dot{\alpha}_i\left(\mathbf{1}-\boldsymbol{B}_i\right)\right\}^s\left(\mathbf{1}-\boldsymbol{B}_i\right)^*\right\}^s-\left\{\left(\mathbf{1}+\boldsymbol{B}_i\right)^*\left\{\boldsymbol{K}_\alpha^{-1}\left(\mathbf{1}+\boldsymbol{B}_i\right)\alpha_i\dot{\boldsymbol{B}}_i\right\}^s\left(\mathbf{1}-\boldsymbol{B}_i\right)^*\right\}^s$$
$$-\left\{\left(\mathbf{1}+\boldsymbol{B}_i\right)^*\left\{\boldsymbol{K}_\alpha^{-1}\left(\mathbf{1}+\boldsymbol{B}_i\right)\alpha_i\left(\mathbf{1}-\boldsymbol{B}_i\right)\right\}^s\left(\dot{\boldsymbol{B}}_i\right)^*\right\}^s$$

References

[1] De Queiroz M S, Kapila V and Yan Q. Adaptive Nonlinear Control of Multiple Spacecraft Formation Flying. *Journal of Guidance, Control, and Dynamics*, Vol. 23, No. 3, pp 385–390, 2000.

[2] Wang J, Liang H, Sun Z, Zhang S and Liu M. Finite-Time Control for Spacecraft Formation with Dual-Number-Based Description. *Journal of Guidance, Control, and Dynamics*, Vol. 35, No. 3, pp 950–962, 2012.

[3] Kristiansen R, Nicklasson P J and Gravdahl J T. Spacecraft Coordination Control in 6DOF: Integrator Backstepping Vs Passivity-Based Control. *Automatica*, Vol. 44, No. 11, pp 2896–2901, 2008.

[4] Wang J and Sun Z. 6-DOF Robust Adaptive Terminal Sliding Mode Control for Spacecraft Formation Flying. *Acta Astronautica*, Vol. 73, pp 76–87, 2012.

[5] Huang Y, Jia Y and Matsuno F. Robust H∞ Control for Spacecraft Formation Flying with Coupled Translational and Rotation Dynamics. *2016 American Control Conference*, Boston, MA, USA, pp 4059–4064, 2016.

[6] Sun R, Wang J, Zhang D, Jia Q and Shao X. Roto-Translational Spacecraft Formation Control Using Aerodynamic Forces. *Journal of Guidance, Control, and Dynamics*, Vol. 40, No. 10, pp 2556–2568, 2017.

[7] Ye D, Zhang J and Sun Z. Extended State Observer–Based Finite-Time Controller Design for Coupled Spacecraft Formation with Actuator Saturation. *Advances in Mechanical Engineering*, Vol. 9, No. 4, pp 1–13, 2017.

[8] Gao C, Yuan J and Zhao Y. ADRC for Spacecraft Attitude and Position Synchronization in Libration Point Orbits. *Acta Astronautica*, Vol. 145, pp 238-249, 2018.

[9] Liu R, Cao X, Liu M and Zhu Y. 6-DOF Fixed-Time Adaptive Tracking Control for Spacecraft Formation Flying with Input Quantization. *Information Sciences*, Vol. 475, pp 82–99, 2019.

[10] Ren W and Cao Y. *Distributed Coordination of Multi-agent Networks*. 1st edition, Springer, 2011.

[11] Ren W. Formation Keeping and Attitude Alignment for Multiple Spacecraft through Local Interactions. *Journal of Guidance, Control, and Dynamics*, Vol. 30, No. 2, pp 633–638, 2007.

[12] Huang X, Yan Y, Zhou Y and Yang Y. Dual-Quaternion Based Distributed Coordination Control of six-DOF Spacecraft Formation with Collision Avoidance. *Aerospace Science and Technology*, Vol. 67, pp 443–455, 2017.

[13] Shasti B, Alasty A and Assadian N. Robust Distributed Control of Spacecraft Formation Flying with Adaptive Network Topology. *Acta Astronautica*, Vol. 136, pp 281–296, 2017.

[14] Zhang J, Ye D, Biggs J D and Sun Z. Finite-Time Relative Orbit-Attitude Tracking Control for Multi-Spacecraft with Collision Avoidance and Changing Network Topologies. *Advances in Space Research*, Vol. 63, No. 3, pp 1161–1175, 2019.

[15] Huang Y and Jia Y. Adaptive Finite Time Distributed 6-DOF Synchronization Control for Spacecraft Formation without Velocity Measurement. *Nonlinear Dynamics*, Vol. 95, No. 3, 2275–2291, 2019.

[16] Arcaute E, Lasenby A and Doran C. Twistors in Geometric Algebra. *Advances in Applied Clifford Algebras*, Vol. 18, pp 373–394, 2008.

[17] Deng Y and Wang Z. Modeling and Control for Spacecraft Relative Pose Motion by Using Twistor Representation. *Journal of Guidance, Control, and Dynamics*, Vol. 39, No. 5, pp 1144–1151, 2016.

[18] Deng Y, Wang Z and Liu L. Unscented Kalman Filter for Spacecraft Pose Estimation Using Twistors. *Journal of Guidance, Control, and Dynamics*, Vol. 39, No. 8, pp 1844–1856, 2016.

[19] Li Q, Liu L, Deng Y, Tang S and Zhao Y. Twistor-Based Synchronous Sliding Mode Control of Spacecraft Attitude and Position[J]. *Chinese Journal of Aeronautics*, Vol. 31, No. 5, pp 1153–1164, 2018.

[20] Zhang B and Cai Y. Twistor-Based Pose Control for Asteroid Landing with Path Constraints. *Nonlinear Dynamics*, Vol. 100, No. 3, pp 2427–2448, 2020.

[21] Filipe N and Tsiotras P. Adaptive Position and Attitude-Tracking Controller for Satellite Proximity Operations Using Dual Quaternions. *Journal of Guidance, Control, and Dynamics*, Vol. 38, No. 4, pp 566–577, 2015.

[22] Wang W, Li C, Sun Y and Ma G. Distributed Coordinated Attitude Tracking Control for Spacecraft Formation with Communication Delays. *ISA Transactions*, Vol. 85, pp 97–106, 2019.

[23] Khalil H K. *Nonlinear Systems*. 3rd edition, Prentice Hall, 2002.

[24] Shtessel Y, Edwards C, Fridman L and Levant A. *Sliding Mode Control and Observation*. 1st edition, Springer, 2014.